Surface Phase Behavior and Surface Tension Evolution for Lysozyme Adsorption onto Clean Interfaces and into DPPC Monolayers: Theory and Experiment

Sekhar Sundaram,† James K. Ferri,† Dieter Vollhardt,‡ and Kathleen J. Stebe*,†

Department of Chemical Engineering, The Johns Hopkins University, Baltimore Maryland 21218, and Max-Planck-Institut für Kolloid- und Grenzflächenforschung, Rudower Chaussee 5, D-12489 Berlin, Germany

Received June 24, 1997. In Final Form: December 16, 1997

The surface phase behavior of lysozyme is studied, first by studying its adsorption at aqueous−gas interfaces and then by studying its penetration into an insoluble monolayer of dipalmitoylphosphatidylcholine (DPPC). When lysozyme adsorbs on an aqueous−gas interface, the surface tension remains constant over an extended period of time before reducing. This induction period indicates a first-order transition at the interface from a surface gaseous phase to a liquid-expanded phase. The coexistence of these phases is demonstrated by fluorescence imaging. The surface tension evolution is compared favorably to theoretical traces predicted for the dynamic adsorption of a soluble amphiphile which undergoes a surface phase change. Lysozyme is an ellipsoidal molecule which can adsorb in either side-on or end-on configurations. The transition from side-on to end-on adsorption is shown to coincide with the phase change. The time scales for the adsorption process are in agreement with a diffusion-controlled mechanism at dilute concentrations but are far longer at elevated concentrations, indicating the presence of a strong kinetic barrier to adsorption. Long time surface tension data as a function of bulk concentration C_∞ show no reduction for C_∞ corresponding to (side-on) gaseous surface states, strong reduction at C_∞ corresponding to (end-on) liquid-expanded surface states. In the penetration experiments, an insoluble monolayer of DPPC is initially present. The surface pressure rise upon exposing the monolayer to lysozyme solution has no induction period. This is explained in terms of the lipid screening cohesive interactions between the adsorbed lysozyme molecules, eliminating the phase change. Finally, Brewster angle microscopy (BAM) images and compression isotherms for the two-component system are discussed in terms of intermolecular interactions.

1. Introduction

When lysozyme adsorbs onto a freshly created aqueous−gas interface, the surface tension remains constant during an induction period. Thereafter, the surface tension reduces. The induction period decreases with bulk concentration. This induction period has been observed in a several protein adsorption studies. Tripp *et al.*[1] studied the dynamic surface tension of lysozyme adsorption using a pendant bubble technique; it was suggested that the induction period in the surface tension may reflect a conformational change at the interface. Van der Vegt *et al.*[2] used sessile drops to simultaneously study the aqueous−gas and aqueous−solid interface of protein solution droplets deposited on Teflon. They report an induction period in both the surface tensions of aqueous−air and aqueous−solid (as inferred from contact angle data) interfaces for a series of proteins, including lysozyme. They attribute the induction period to conformational changes of the adsorbed protein or suggest that the excess surface concentration may be zero during this period. Serrein *et al.*[3] observed an induction period for the proteins casein and buttermilk. They assumed that protein adsorption can be neglected during this time period and shifted the origin of the time axis accordingly. Graham and Phillips[4] reported both the dynamic surface pressure by Wilhelmy plate technique and the surface concentration evolution using radiolabeling techniques for lysozyme. While the surface pressure does not change initially, the surface concentration does. A similar study of the surface concentration, with careful corrections for the adsorption of lysozyme to the bounding surfaces of the experimental apparatus, was performed by Hunter *et al.*[5] Again, in their data, there is no delay in the adsorption of lysozyme at the aqueous−air interface.

Xu and Damodaran[6] also used radiolabeling to study lysozyme adsorption and a Wilhelmy plate to study the surface tension. They report a delay in the onset of adsorption after aspirating the interface to remove any preadsorbed protein, contrary to the results of Hunter *et al.* and Graham and Phillips. Xu and Damodoran also report that the surface pressure increase lags the surface concentration and suggest that lysozyme does not alter the forces at the interface until some degree of conformational change has occurred there.

Induction periods in the surface tension relaxation have been observed for simple surface active molecules such as the long chain 1-alcohols, e.g., 1-decanol, whose structure favors cohesive intermolecular interactions. (For a thorough review of other soluble surfactant studies that report

* To whom correspondence should be addressed. E-mail: kjs@jhuvms.hcf.jhu.edu. Telephone: (410) 516-7769. Fax: (410) 516-5510.

† The Johns Hopkins University.

‡ Max-Planck-Institut für Kolloid- und Grenzflächenforschung.

(1) Tripp, B. C.; Magda, J. J.; Andrade, J. D. *J. Colloid Interface Sci.* **1995**, *173*, 16.

(2) Van der Vegt, W.; Norde, W.; Van der Mei, H. C.; Busscher, H. J. *J. Colloid Interface Sci.* **1996**, *179*, 57.

(3) Serrien, G.; Geeraerts, G.; Ghosh, L.; Joos, P. *J. Colloids Surf.* **1992**, *68*, 219.

(4) Graham, D. E.; Phillips, M. C. *J. Colloid Interface Sci.* **1979**, *70*, 403.

(5) Hunter, J. R.; Kilpatrick, P. K.; Carbonell, R. G. *J. Colloid Interface Sci.* **1990**, *137*, 462.

(6) Xu, S.; Damodaran, S. *Langmuir* **1992**, *8*, 2021.

S0743-7463(97)00670-7 CCC: $15.00
Published on Web 03/03/1998

induction times, see Lin *et al.*[7] and Pollard[8] *et al.*) When these interactions are pronounced enough, a 2-D phase transition can occur from a surface gaseous phase to a surface liquid-expanded phase. For 1-decanol, the phase transition occurs when the mean area per molecule is small enough to allow the molecule to contact neighboring molecules in a side-on configuration.[7] Further adsorption is thought to be accompanied by a molecular reorientation to end-on adsorption.

Lysozyme in solution under the conditions of this study (pH = 7.5, 0.15 M NaCl in phosphate buffered saline) has a charge of +8*e*; the Debye length is 7.8 Å. Similar conditions were used in the protein adsorption studies reviewed above. Electrostatic repulsion is effectively screened; the second virial coefficient for lysozyme in solution under similar conditions was measured by osmotic pressure techniques in a study of protein crystallization and found to be negative.[9]

Lysozyme has a hard, ellipsoidal structure which does not denature easily. The molecule has two characteristic cross sections: a side of dimensions of roughly 30 Å × 45 Å and an end of dimension 30 Å × 30 Å.[10] Hunter *et al.* report that lysozyme adsorbs on aqueous−gas interfaces in a side-on configuration at dilute coverages, with a transition to an end-on configuration at more elevated coverages. In this paper, we argue that this reorientation occurs as a first-order surface phase change, causing an induction period to appear in the dynamic surface tension. Consider adsorption to an interface that is exposed to a lysozyme solution. Lysozyme initially adsorbs in the surface gaseous, side-on configuration. The surface tension barely reduces. Adsorption decreases the area/molecule, driving the protein from the surface gaseous state to a coexistence state, in which the molecules reorient from side-on (the gaseous state) to end-on (the liquid-expanded state). For a first order transition, this occurs at constant surface tension. Domains of end-on lysozyme grow as the adsorption proceeds until they cover the interface. Further adsorption of lysozyme occurs in the end-on, liquid-expanded state, for which the surface tension is highly sensitive.

To probe whether domains of liquid-expanded phase indeed form, we spread a fluorescent dye from chloroform at the interface of a lysozyme solution. As lysozyme adsorbed, fluorescence images of liquid-expanded domains are apparent in a dark surface gaseous phase, suggesting that a surface phase transformation is indeed occurring (see Figure 1).

In this study, the surface phase behavior of lysozyme adsorption is addressed. Using both pendant bubble tensiometry and the Wilhelmy plate technique, the dynamic surface tension behavior of air−lysozyme solution interfaces is carefully studied. The experiments were performed in controlled environments to prevent any artifacts caused by convection or evaporation. This system fails to equilibrate after extremely long times (e.g. even after 10^5 seconds, lysozyme solutions of concentrations C_∞ of 9.2×10^{-4} wt % have not yet equilibrated). The profile shapes are qualitatively similar to those predicted by a dynamic Frumkin adsorption model with cohesive interactions strong enough to drive a surface phase transition.[11] They are discussed in this context.

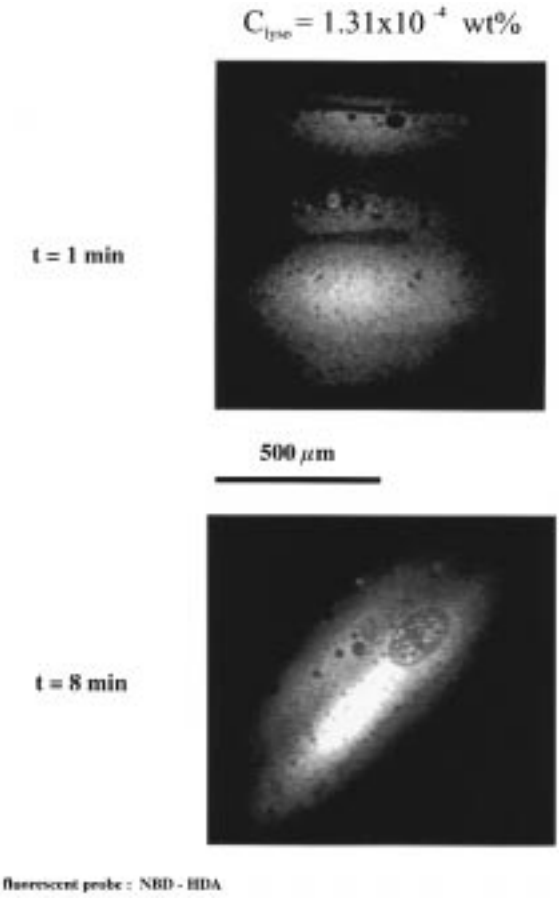

Figure 1. Fluorescence images of liquid-expanded islands of lysozyme in a surface gaseous phase for lysozyme adsorbed from solution. The fluorescent dye is NBD−HDA, (4-hexadecylammonio)-7-nitrobenz-2-oxa-1,3-diazole, from Molecular Probes. The dye was excited by a 10 mW argon ion laser at 488 nm. The dye is quenched in the gaseous phase and fluoresces in the liquid-expanded phase.

The long time surface tension data reported as a function of C_∞ can be divided into three regions which correspond to different configurations of adsorbed lysozyme as described by Hunter *et al.*[5] For C_∞ values that are sufficiently dilute, the surface tension remains equal to that for the pure buffer. This concentration range corresponds to that for side-on adsorption. For greater C_∞, the surface tension reduces strongly for concentrations corresponding to end-on adsorption. Finally, the surface tension again remains constant for C_∞ corresponding to multilayer formation.

Proteins have been shown to have adsorption[12] and desorption[4,5] kinetic barriers. Using a simple scaling argument, it is shown that the surface tension data for lysozyme agrees with a diffusion-controlled mechanism for dilute concentrations but shifts to strong kinetic control at higher concentrations.

The phase change is driven by cohesive interactions between the lysozyme molecules. These interactions are altered by the presence of a second surface active component. For example, the induction period in surface tension disappears when lysozyme adsorbs onto an interface initially covered with an insoluble monolayer of DPPC.[13] The presence of DPPC may screen the cohesion

(7) Lin, S. Y.; McKeigue, K.; Maldarelli, C. *Langmuir* **1991**, *7*, 1055.
(8) Pollard, M. L.; Pan, R.; Steiner, C.; Maldarelli, C. Submitted to *Langmuir*.
(9) Rosenbaum, D. F.; Zukoski, C. F. *J. Cryst. Growth* **1996**, *169*, 752.
(10) Imoto, T.; Johnson, L. N.; North, A. C. T.; Phillips, D. C.; Rupley, J. A. *Enzymes* **1970**, *7*, 665.
(11) Ferri, J. K.; Stebe, K. J. Submitted to *J. Colloid Interface Sci.*
(12) See, for example: MacRitchie, F.; Alexander, A. E. *J. Colloid Sci.* **1963**, *18*, 453. MacRitchie, F.; Alexander, A. E. *J. Colloid Sci.* **1963**, *18*, 458. MacRitchie, F.; Alexander, A. E. *J. Colloid Sci.* **1963**, *18*, 464.
(13) Sundaram, S.; Stebe, K. J. *Langmuir* **1997**, *13*, 1729.

between the adsorbed lysozyme and can prevent a phase change. This is shown using a two-component Frumkin model.

Finally, the impact of lysozyme on the phase behavior of a DPPC monolayer is investigated. A compression isotherm of DPPC taken on the surface of a lysozyme solution is discussed. Using Brewster angle microscopy (BAM),[14,15] images are recorded of domains formed in the mixed monolayer for DPPC initially in the coexistence region between the liquid-expanded to liquid-condensed states. The images show that the domain morphology and the orientational order in the domains differ from those that occur in the absence of lysozyme.

2. Experimental Section

In this paper, three sets of experiments are presented: (i) the surface tension relaxation caused by lysozyme adsorption at aqueous−gas interfaces by pendant bubble and Wilhelmy plate methods; (ii) the dynamic surface pressure increase driven by lysozyme penetration into an insoluble monolayer of DPPC; (iii) a study of the morphology and inner structure of DPPC domains in the presence of adsorbed lysozyme by BAM. The materials and experimental protocols for each experiment are described below.

2.1. Materials. All chemicals were purchased from Sigma chemicals and used without further modification, including chicken egg lysozyme, L-DPPC, and chloroform. The DPPC was spread from chloroform. All experiments were done in a phosphate buffered saline solution at pH 7.4 and 0.15 M NaCl. Pure water from a Millipore Milli-Q water filtration system with a resistivity of 18 MΩ cm was used to make all solutions and for all cleaning procedures. Lysozyme solutions were stored at 5 °C and were used within 3 days or discarded.

Scrupulous cleaning of all apparatus was performed. The quartz cell used in the pendant bubble experiments and the Teflon beakers for the lysozyme experiments were cleaned in Nochromix acid solution and rinsed copiously in the purified water. Prior to each experiment, the Langmuir troughs were filled with boiling water and soaked for an hour. The water was then removed by suction, and the trough was carefully wiped with either benzene or hexane. The trough was then soaked again in hot water. The Wilhelmy plates used to monitor the surface pressure in the monolayer penetration experiments were made of glass; they were cleaned by soaking them in a bath of sulfuric acid and then rinsing copiously. The Wilhelmy plates used to study the lysozyme adsorption at air−buffer interfaces were made of platinum; they were cleaned by "flaming" them before each experiment.

2.2. Surface Tension Relaxation Studies. Two techniques were used to study the surface tension relaxation of lysozyme at aqueous−air interfaces. The protocol for each is standard, and is discussed briefly below. All experiments were performed at 22 ± 1 °C.

Wilhelmy Plate. The surface tension relaxation of lysozyme was studied by the Wilhelmy plate technique. The force transducer was calibrated with the weight of the plate in air. The weight of the meniscus was then recorded. Assuming zero contact angle, the meniscus weight was then related to the surface tension.

The Wilhelmy plate was configured so that it hung directly above a Teflon beaker. Aqueous solutions of lysozyme of known concentration were poured into the beaker; the liquid level was raised until the solution came into contact with the Wilhelmy plate edge so that a meniscus formed. A typical elapsed time between pouring and contact of the liquid with the plate is about 30 s. The force transducer was configured to a PC; the surface tension was recorded continuously throughout the experiment.

The force transducer and beaker were housed in a tightly sealed environmental chamber, minimizing evaporation. The temperature was also monitored and recorded to disk throughout the adsorption process. The experiments typically lasted several days. Temperature variations were less than ±1 °C. The error bar in our Wilhelmy plate measurements is ±0.5 dyn/cm.

Pendant Bubble Method. The pendant bubble apparatus design, experimental protocol, and data analysis have been described in detail elsewhere[16] and are only briefly reviewed here.

An optical quality quartz cell filled with lysozyme solution was placed in the path of a collimated light beam. An inverted needle was immersed in the solution. At the needle tip, a pendant bubble was formed. The light beam cast a silhouette of the bubble onto a CCD camera, allowing a digitized image of the bubble to be recorded; this image was stored via a digitizer on a PC. These digital images were processed using an edge detection routine that locates the bubble edge precisely, to within fractions of pixels, using an interpolation routine. The bubble edge was numerically compared to the shape predicted by the Young−Laplace equation for a given surface tension according to the protocol presented in Rotenberg *et al.*[17]

Prior to each experiment, the surface tension of clean water was confirmed at the laboratory temperature. CRC handbook[18] values are recovered within 0.2 dyn/cm, or the apparatus is recalibrated.

The apparatus requires careful calibration, and thereafter gives highly reproducible, precise results. Collimating lenses are aligned. The calibration routine involves finding two independent aspect ratios. One is the ratio of pixels per unit length. The other is the ratio of x to y pixels. These ratios are obtained from a digitized image of a spherical bead. Once calibrated, the system is stable; recalibration is required only if the lenses inadvertently become misaligned.

The inverted needle was attached to a solenoid valve−syringe pump assembly interfaced to a PC via an A/D board. This assembly allowed bubbles of constant mass to be formed and subsequently isolated from the surrounding environment. By pressurization of the air in the syringe and rapid opening and closing of the solenoid valve, bubbles can be formed reproducibly in as little as 0.05 s, allowing early-time surface tension to be measured.

In each experiment, a pendant bubble was formed. As protein adsorbed on the interface, the surface tension decreased and the bubble became increasingly distended. By recording of the bubble image over time, the evolution of the surface tension was determined.

2.3. Monolayer Penetration Trough. The circular trough apparatus has been described in detail elsewhere,[19] and is only briefly described here (see Figure 2). A circular trough was partitioned into two semicircular halves by two fixed barriers (A). Region I of the trough was filled with pure buffer solution and region II by buffered lysozyme solution. Both regions I and II were aspirated prior to the deposition of DPPC on region I. Apart from the fixed dividing barriers, there were two more barriers which sweep the interface (B). The DPPC monolayer was formed in region I between the two sweeping barriers. These barriers were used to compress the DPPC monolayer to the desired surface pressure at an average rate of 140 pm^2/molecule/s. Immediately after compressing the monolayer, it was moved from region I to region II at constant area, exposing the monolayer to the surface active lysozyme. The surface pressure was monitored by a Wilhelmy plate during and after the transfer process.

One advantage of this protocol is that the insoluble monolayer is exposed to the soluble amphiphile with a minimum of disruption by convection (in comparison to methods where the soluble component is injected into the subphase). The initial conditions are well-defined. However, because of the large surface area of the trough, evaporation of the subphase was significant in experiments that lasted several hours.

2.4. BAM Study of DPPC−Lysozyme System. A Brewster angle microscope[20] (BAM 1, NFT, Göttingen) was mounted on

(14) Hönig, D.; Möbius, D. *Thin Solid Films* **1992**, *210/211*, 64.
(15) Henon, S.; Meunier, J. *J. Chem. Phys* **1993**, *98*, 9148.
(16) Johnson, D. O.; Stebe, K. J. *J. Colloid Interface Sci.* **1996**, *182*, 526.
(17) Rotenburg, Y.; Boruvka, L.; Neumann, A. W. *J. Colloid Interface Sci.* **1983**, *93*, 169.
(18) *CRC Handbook of Chemistry and Physics*, 72nd ed.; CRC Press: Boca Raton, FL, 1991; p **6**-9.
(19) Vollhardt, D. *Mater. Sci. Forum* **1988**, *25*, 541.

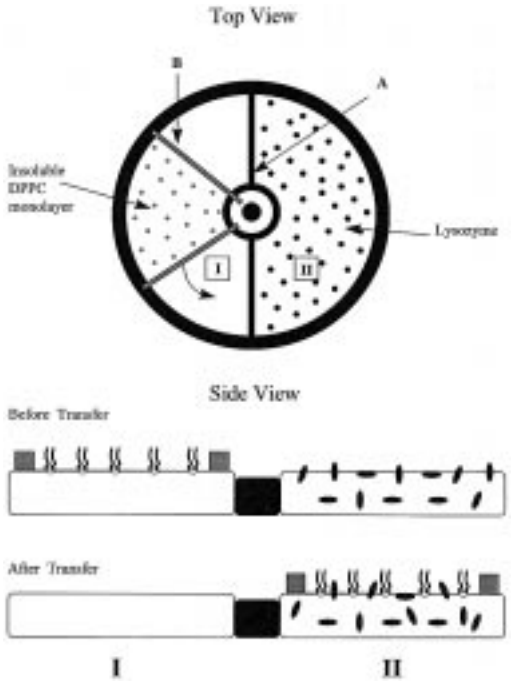

Figure 2. Schematic of the monolayer penetration trough used in the dynamic penetration experiment. Region I contains pure phosphate buffer solution. The insoluble monolayer, DPPC, is spread on region I and compressed to desired surface pressure, before it is swept to region II. Region II is filled with buffered lysozyme solution.

a Langmuir trough. Immediately after sweeping the interface, a DPPC monolayer was spread from chloroform on the surface of a buffered lysozyme solution. The monolayer was then compressed slowly, at a rate of 0.5 Å^2 molecule^{-1} min^{-1} to 68 nm^2/molecule DPPC, in the plateau region for coexistence of LE−LC phases. BAM images of the domains formed were obtained using a CCD camera and video recorder. The evolution of these domains was studied at two lysozyme concentrations (5×10^{-5} wt % and 10^{-4} wt %).

3. Results: Surface Tension

3.1. Surface Tension Relaxation. In Figure 3, a family of surface tension relaxation curves obtained by the pendant bubble method for lysozyme as a function of concentration is shown. The bulk concentrations for all three experiments correspond to a final state of end-on adsorption, according to Hunter *et al.*'s data. There is a prolonged induction period over which the surface tension remains constant, roughly 8000 s for the most dilute solution ($C_\infty = 4.8 \times 10^{-5}$ wt %), and 700 s for the more concentrated solution, ($C_\infty = 1.0 \times 10^{-3}$ wt %). The time scales for the entire relaxation process were prohibitively long for the pendant bubble method; typically, the bubble popped while the surface tension was still strongly decreasing with time. (The data reported in Figure 3c are complex; two long-lived plateaus are apparent in the long time data, suggesting that there may be first-order phase changes occurring in the interface caused by rearrangements at long times. These plateaus are reproducible; they are also apparent in the Wilhelmy plate data reported at a similar concentration in Figure 5.)

The Wilhelmy plate technique allowed the long time surface tension to be studied. Dynamic traces of the surface tension were recorded for greater than 10^5 s; typical data are presented in Figures 4 and 5 as a function of

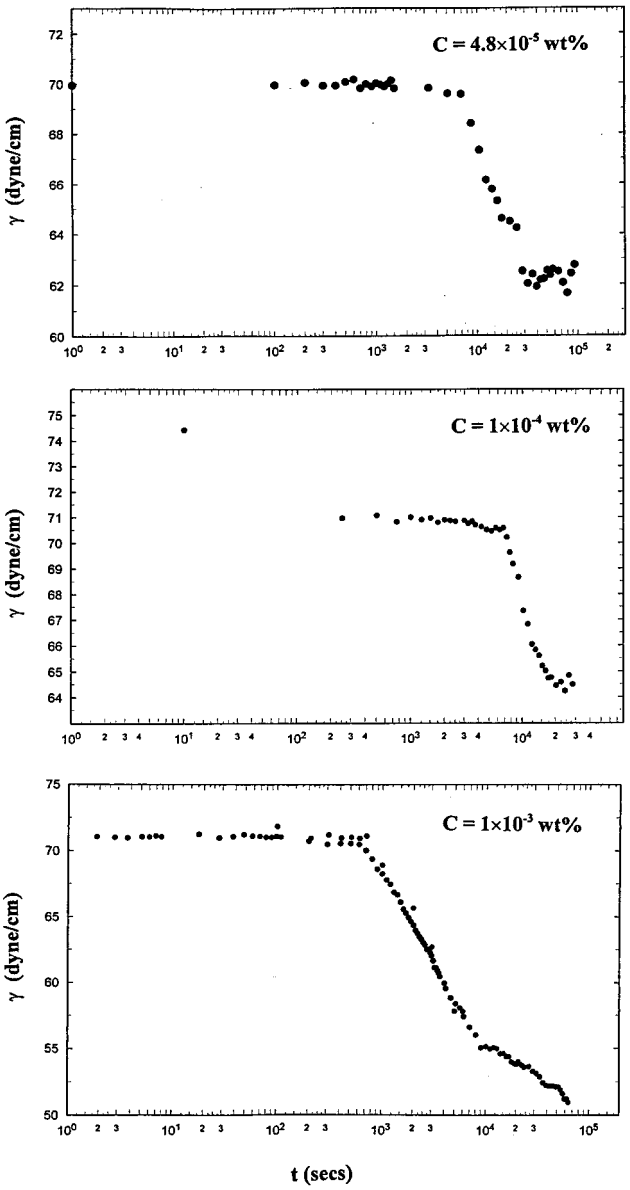

Figure 3. Dynamics of surface tension decrease of lysozyme obtained by the pendant bubble for (a) $C = 4.8 \times 10^{-5}$ wt %, (b) $C = 1.08 \times 10^{-4}$ wt %, and (c) $C = 1.00 \times 10^{-3}$ wt %. These bulk concentrations correspond to a final state of end-on adsorption.

concentration. These experiments were terminated after there was no apparent change in the surface tension after 1 day.

Figure 4 corresponds to a bulk lysozyme concentration of side-on final adsorbed state according to Hunter *et al.*'s data. The surface tension for this experiment does not change even after 2−3 days; the interface never leaves the surface gaseous state.

In Figure 5, the bulk concentrations correspond to a final state of end-on adsorption; they are similar to the data reported in Figure 3. Note that from the shape of the surface tension profiles graphed against log *t*, it is clear that the traces in Figures 3 and 5 have not attained equilibrium. This calls into question any discussions of liquid−gas equilibrium surface tensions for this protein, such as those in Graham and Phillips. Xu and Damodoran also report that the surface tension of lysozyme fails to equilibrate after up to 24 h. Here it is shown that, even after several days, no equilibrium is attained.

(20) Vollhardt, D. *Adv. Colloid Interface Sci.* **1996**, *64*, 143.

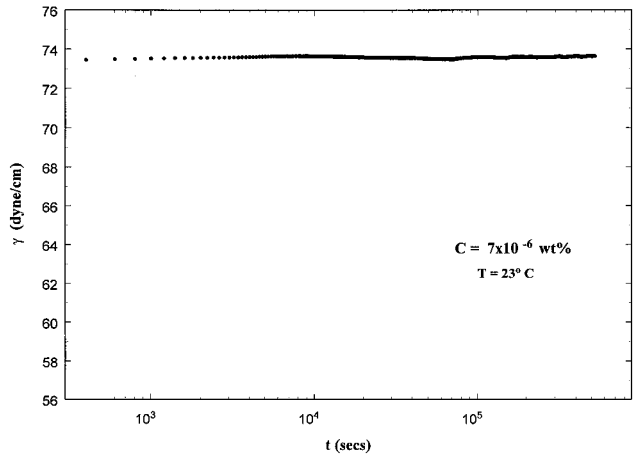

Figure 4. Dynamics of surface tension decrease of lysozyme obtained on the Wilhelmy plate for $C = 7 \times 10^{-6}$ wt %. Bulk concentration correspond to a final state of side-on adsorption.

3.2. Solution Age and Reproducibility. Most of our experiments lasted 3−4 days, all at 22 ± 1 °C. None were run beyond 5 days. Typically, protein solutions were gently stirred overnight (a maximum of 10 h) before the experiments were initiated. The following control experiments were performed (all at 22 ± 1 °C).

A circular dichroism (CD) absorption spectrum was obtained for a lysozyme solution of concentration 3.53×10^{-3} wt % that was aged for 2 days and compared to a reference lysozyme control sample of the same concentration. (The control sample was well characterized by a calorimetric technique and by CD spectra.) The spectra nearly superpose (Figure 6a), suggesting that the lysozyme is pure and in its native state.

To assess the impact of aging on our experiments, a protein solution of 2.2×10^{-4} wt % was prepared by our usual protocol; it was stored at 22 ± 1 °C in a sealed volumetric flask. The same solution was used for all of the control experiments discussed below. The duration of the induction period t_{ind} was checked as a function of the solution age, 200 mL of solution was poured into a Teflon beaker, and the surface tension evolution was studied using the Wilhelmy plate technique. The induction period lasts roughly 4×10^4 s at this concentration, one of the longest induction periods reported.

The duration t_{ind} is reported in Figure 6b; it showed little change for 2 days (day 1, $t_{ind} = 4 \times 10^4$ s; day 2 $t_{ind} = 4 \times 10^4$ s). However, by the fourth day, the duration deceased significantly (day 4, $t_{ind} = 9 \times 10^3$ s). This cannot be explained by a depletion of the bulk concentration by adsorption to the sides of the flask or beaker, which would increase t_{ind}. It may indicate protein denaturation. All induction periods reported above occur within the time span during which these control experiments indicate reproducibility. The longer time data should be interpreted cautiously, noting the possibility of denaturation.

3.3. Long Time Surface Tension Data. Long time surface tension data as a function of lysozyme bulk concentration is shown in Figure 7. The data show differing behavior in the three characteristic regions reported by Hunter *et al.* in their adsorption isotherm. At dilute bulk concentrations, lysozyme adsorbs in a surface gaseous (side-on) state where the surface tension decreases negligibly. In the second region, which corresponds to the liquid-expanded phase, the surface tension is very sensitive to the bulk concentrations. At high bulk concentrations, multilayers form; the surface tension does not change appreciably with bulk concentration. The dashed lines indicate the transition between side-on to end-on adsorption, and end-on to multilayer adsorption, according to Hunter *et al.*

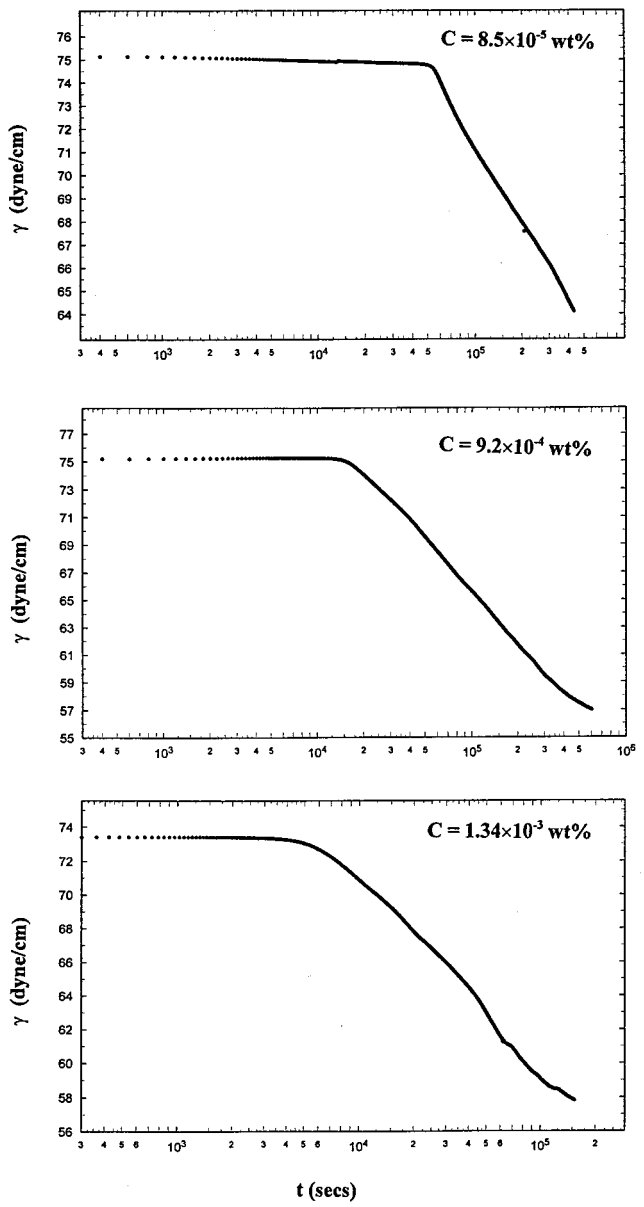

Figure 5. Dynamics of surface tension decrease of lysozyme obtained on the Wilhelmy plate for (a) $C = 8.5 \times 10^{-5}$ wt %, (b) $C = 9.2 \times 10^{-4}$ wt %, and (c) $C = 1.34 \times 10^{-3}$ wt %. These bulk concentrations correspond to a final state of end-on adsorption.

In all of the Wilhelmy plate experiments and in one of the pendant bubble studies, the surface tension immediately after the interface is formed is higher than that for clean water (72.6 dyn/cm at 22 °C according to the *CRC Handbook*). This elevation in surface tension may be caused by the surface depletion of the ions and charged proteins from the interface at early times.[21] The surface tension was also higher than the pure water value for the entire surface tension trace of surface gaseous lysozyme in Figure 4 and for pure buffer (not shown).

3.4. Monolayer Penetration. In parts a and b of Figure 8, data are presented for lysozyme penetration

(21) See, for example: Adam, N. K. *The Physics and Chemistry of Surfaces*, 3rd ed.; Oxford Press: Cambridge, England, 1946. Davies J. T.; Rideal, E. K. *Interfacial Phenomena*; Academic Press: New York, 1961. Adamson, A. W. *Physical Chemistry of Surfaces*; John Wiley and Sons: New York, 1990. Hiemenz, P. C. *Principles of Colloid and Surface Chemistry*; Marcel Dekker: New York, 1986.

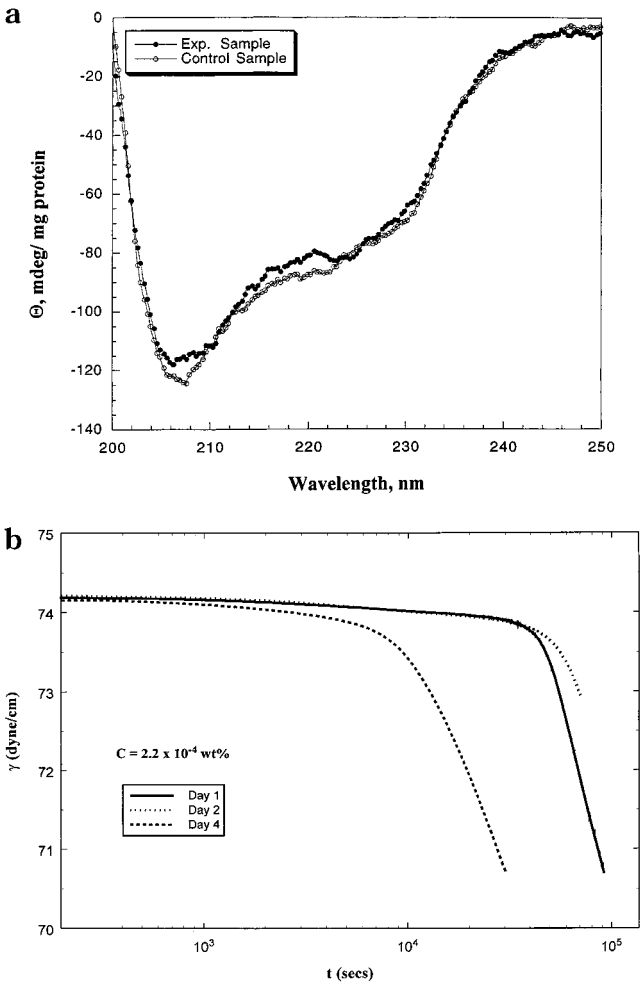

Figure 6. (a) Circular dichroism (CD) spectra of a lysozyme solution of concentration 3.53×10^{-3} wt % used in our experiments compared to a control sample of the same concentration. The control sample of lysozyme was characterized by the standard calorimetric technique and by CD spectra. (b) Surface tension relaxation of a lysozyme solution of concentration 2.2×10^{-4} wt % measured on different days.

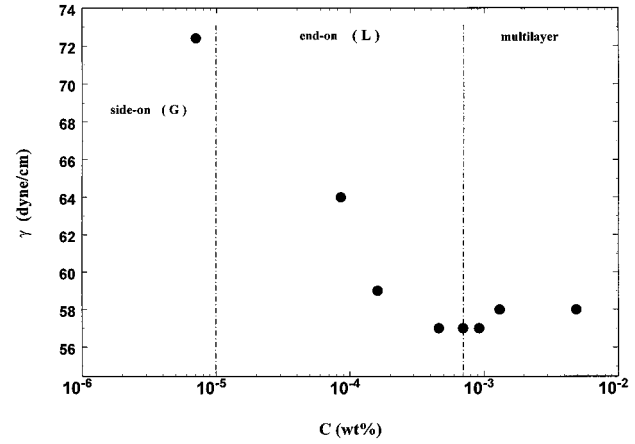

Figure 7. Long time surface tension data as a function of lysozyme bulk concentration obtained by using Wilhelmy plate. Here the dotted lines indicate the transition between side-on (G) to end-on (L) and end-on (L) to multilayer adsorption according to Hunter *et al.*

into a DPPC monolayer for bulk lysozyme concentration, 3×10^{-5} wt %. The two graphs correspond to $x_1 = 0$ (no DPPC) and $x_1 = 0.44$ ($\pi(t = 0) = 3.4$ dyn/cm at 91 Å^2/

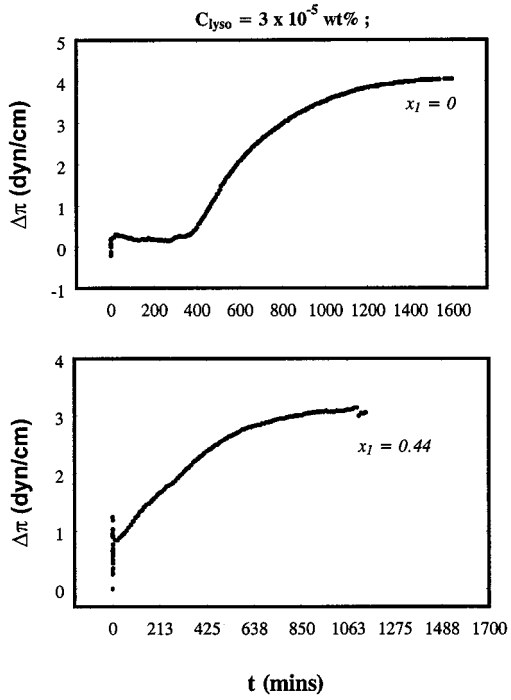

Figure 8. Dynamics of surface pressure increase of lysozyme obtained on the circular multi-compartment trough for (a) $C = 3.0 \times 10^{-5}$ wt %, for $x_1 = 0.0$, and (b) $C = 3.0 \times 10^{-5}$ wt %, for $x_1 = 0.44$.

molecule). (These data were presented as Figure 8 in Sundaram and Stebe,[13] where the role of the lipid in rendering diffusion time scales more rapid was discussed. Here, the focus is the surface phase behavior.) The induction period is clearly apparent in the absence of DPPC, and disappears when DPPC is present. This occurred in all lysozyme−DPPC experiments that were performed. This may be caused by the screening of cohesive interactions among the adsorbed lysozyme molecules by DPPC, which can suppress the phase transition, as discussed below.

4. Comparison of Theory and Experiment

4.1. Surface Phase Transitions of a Soluble Amphiphile. The interpretation of the induction period as a surface tension relaxation was first put forth by Lin *et al.* The analysis of these induction times in terms of surface binodal compositions located via a Maxwell construction on the surface equation of state is discussed by Ferri and Stebe.[11] The key ideas are briefly reviewed here and subsequently extended to a two-component monolayer.

Equilibrium. The Frumkin isotherm is an adsorption site model which accounts for interactions between adsorbed molecules. It is given by

$$x = \frac{k}{k + \exp(Kx)} \tag{1}$$

where

$$x = \frac{\Gamma_{eq}}{\Gamma_\infty}; \quad k = \frac{C_\infty}{a}; \quad a = \frac{\alpha}{\beta} \tag{2}$$

In these expressions, the equilibrium surface concentration is denoted by Γ_{eq}, the maximum surface packing by Γ_∞. Their ratio is x, the fraction of interface occupied by the adsorbed molecule at equilibrium. The bulk concen-

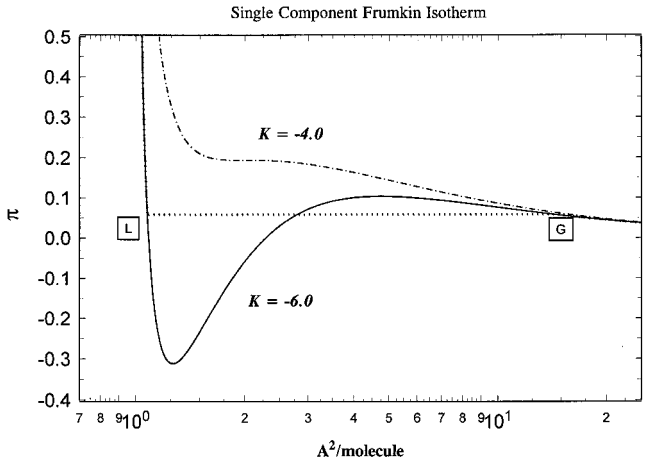

Figure 9. Graph of surface pressure, π, as a function of area/molecule for the Frumkin isotherm for a single amphiphile under critical conditions ($K = -4$) and conditions for which a surface phase change is realized ($K = -6$). The surface binodals are demarcated by the symbol G for the gaseous state and L for the liquid-expanded state.

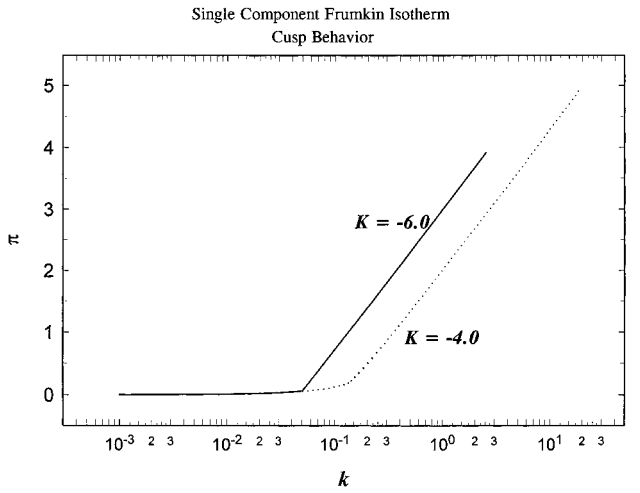

Figure 10. Graph of surface pressure, π, as a function of dimensionless bulk concentration, k for $K = -6$. The critical bulk concentration for which the two surface phases coexist is located at the cusp.

tration of the adsorbing species is denoted by C_∞. The parameter a is a measure of the surface activity of the molecule; the greater is $1/a$, the greater the tendency of the molecule to partition to the interface. The ratio of C_∞/a is the adsorption number k. The parameter K can be related to the energy of interaction between adsorbed molecules in a lattice site model. In a reaction kinetic model, K can be interpreted as the differences in the slopes of the activation energies for adsorption and desorption with respect to the surface concentration. It is a measure of intermolecular interactions; for cohesive interactions, $K < 0$. The surface equation of state corresponding to the Frumkin isotherm is

$$\pi = \gamma_o - \gamma = -RT\Gamma_\infty\left[\ln(1-x) - \frac{K}{2}x^2\right] \qquad (3)$$

where γ is the surface tension in equilibrium with Γ_{eq}, γ_o is the surface tension of the clean aqueous−air interface, and π is the surface pressure. For $K = -4$ and $x = 1/2$ the system exhibits critical behavior. This corresponds to the cohesive energies between the molecules being equal in magnitude to the thermal energy k_BT, where k_B is the Boltzmann constant. For larger cohesive interactions (i.e. $K < -4$), a surface phase transition is realized.

For $K < -4$, the surface separates into a coexisting surface gaseous (G) and surface liquid-expanded (L) phases. The surface pressure is graphed as a function of $1/x$ in Figure 9. The spinodal points separating unstable states from stable/metastable states are located equating $\partial\gamma/\partial\Gamma$ to zero. The tie line location is determined using the Maxwell rule. The endpoints of the tieline are the gas binodal surface concentration, Γ_G, and liquid-expanded binodal surface concentrations, Γ_L. For coverages intermediate to these two values, the surface pressure remains constant at the tieline value, and the adsorbent forms domains of concentration Γ_L floating in a surface of concentration Γ_G. In Figure 10, a graph of γ vs dimensionles bulk concentration (k) is presented for $K < -4$. A cusp is apparent at C^c, the bulk concentration in equilibrium with the coexisting surface gaseous and liquid-expanded phases. As discussed in Lin *et al.*, this can be understood in terms of the Gibbs adsorption equation

$$\Gamma = \frac{-1}{RT}\frac{d\gamma}{d(\ln C)} \qquad (4)$$

which states that the slope of the $\gamma-\ln C$ curve is proportional to Γ. At C^c, the surface concentration increases from the gaseous binodal surface coverage Γ_G to the liquid-expanded binodal value Γ_L. This cusp is the signature of a surface phase transition for a bulk soluble surface active molecule.

Evolution of Surface Tension with a Surface Phase Change. To show a dynamic surface tension profile corresponding to the phase change, the mass flux to the interface must be modeled. Here, we assume diffusion control only for the purpose of illustration. (The data, in fact, indicate a strong kinetic barrier to adsorption at elevated concentrations, as discussed below.)

Consider the mass flux to a planar interface freshly formed in a solution containing a surface active molecule at bulk concentration C_∞. Let the surface be initially free of adsorbed surface active component (i.e., lysozyme in this case). The initial and boundary conditions are

$$\lim_{z\to\infty} C(z,t) = C_\infty \qquad (5)$$

$$\Gamma(t=0) = 0$$

$$C(z,t=0) = C_\infty$$

$$C_s(z,t=0) = 0 \qquad (6)$$

where z is the distance away from the interface and t is time. Protein adsorbs and depletes the sublayer concentration $C_s(t)$. This causes protein to diffuse toward the interface. The diffusion flux to the interface establishes $C_s(t)$ according to

$$\frac{d\Gamma(t)}{dt} = D\frac{\partial C}{\partial z}\Big|_{z=0} \qquad (7)$$

In this limit, protein partitions between the sublayer and the interface in local equilibrium. The bulk concentration $C(z,t)$ is determined by Fick's law

$$\frac{\partial C}{\partial t} = D\frac{\partial^2 C}{\partial z^2} \qquad (8)$$

where D is the bulk diffusion coefficient of the protein.

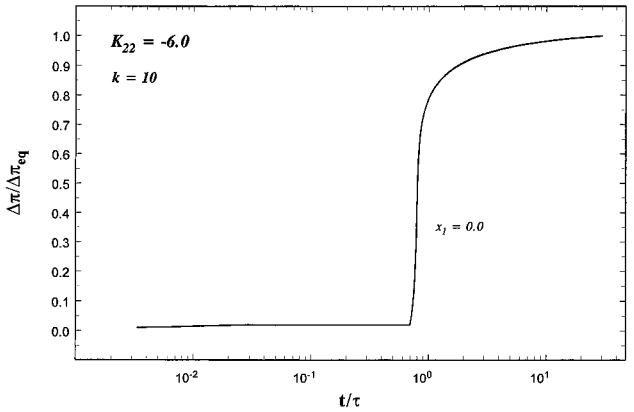

Figure 11. Dynamic surface pressure increase for an amphiphile undergoing a gaseous-liquid-expanded phase change. For this graph, $K = -6$, $k = 10$, and τ is the characteristic diffusion time scale defined as $\tau = h^2/D$ where $h = \Gamma_{eq}/C_\infty$ and D is the diffusion coefficient.

The solution of eqs 5−8 is[22]

$$\Gamma(t) = 2\sqrt{\frac{D}{\pi}}[C_\infty\sqrt{t} - \int_0^{\sqrt{t}} C_s(t-\tau)\, d\sqrt{\tau}] \qquad (9)$$

Equation 9 is solved simultaneously with the instantaneous adsorption isotherm to give $\Gamma(t)$ using standard numerical techniques.[23]

The isotherm that relates $\Gamma(C_s(t))$ is

$$\frac{\Gamma(t)}{\Gamma_\infty} = \left[\frac{C_s(t)}{a\exp\left(K\frac{\Gamma(t)}{\Gamma_\infty}\right) + C_s(t)}\right] \qquad (10)$$

for $C_s(t) < C_c$ or $C_s(t) > C_c$. For $C_s(t) = C_c$, the surface concentration changes by allowing islands of concentration Γ_L to grow at the expense of area covered by Γ_G. That is, the surface undergoes a first-order phase transition in which the sublayer concentration C_s remains constant at C_c. During this time, the diffusion flux remains constant until $\Gamma = \Gamma_L$. Thereafter, the isotherm and eq 9 again determine the surface concentration.

Given $\Gamma(t)$, $\pi(t)$ is given by

$$\pi = -RT\Gamma_\infty\left[\ln\left(1 - \frac{\Gamma(t)x}{\Gamma_{eq}}\right) - \frac{K}{2}\left(\frac{\Gamma(t)x}{\Gamma_{eq}}\right)^2\right] \qquad (11)$$

for $\Gamma(t) < \Gamma_G$ or $\Gamma(t) > \Gamma_L$ and by the tieline value for $\Gamma_G < \Gamma(t) < \Gamma_L$.

Using these equations the dynamic trace of the surface tension (in dimensionless form) is determined. It is shown in Figure 11 for $K = -6$, where time is made dimensionless by the characteristic diffusion time scale $\tau = h^2/D$, where $h = \Gamma_{eq}/C_\infty$. The surface tension exhibits a plateau that corresponds to the adsorption of protein in the gaseous phase and then the coexistence phase. The plateau ends when enough protein has adsorbed that the surface is in a surface liquid-expanded phase.

4.2. Comparison to Lysozyme Surface Tension Data. The model has a continuous flux of protein to the interface, with a monotonically increasing Γ as reported in Graham and Phillips[4] and Hunter *et al.*[5] Simultaneously, the surface tension γ initially remains constant because of the surface phase change, subsequently reducing for $\Gamma > \Gamma_L$. The theoretical surface tension and our experimental curves have the same general shape.

The disparity in the surface tension relaxation time scales obtained by Wilhelmy plate and by pendant bubble (Figures 3 and 5) is a consequence of curvature in a diffusion-dominated system. The diffusion-controlled adsorption to a spherical bubble of radius r_o obeys a modified form of the Ward and Tordai solution[7]

$$\Gamma(t) = \frac{D}{r_o}[C_\infty t - \int_0^t C_s(\tau)\, d\tau] + 2\sqrt{\frac{D}{\pi}}[C_\infty\sqrt{t} - \int_0^{\sqrt{t}} C_s(t-\tau)\, d\sqrt{\tau}] \qquad (12)$$

This is an exact solution for the diffusion-controlled adsorption to a sphere. The first two terms on the right-hand side of eq 12 accounts for the more rapid mass flux to a curved interface; as r_o tends to infinity, the planar solution (eq 9) is recovered.

Consider the right-hand side of eq 12. Note that the first and third terms are the contributions of the forward diffusion process, and the second and fourth terms are back-diffusion contributions. Early in the adsorption process, C_s is small, back diffusion is negligible, and the mass flux to the sphere is faster than that to a plane by the first term. In our experiments, the effect of curvature is most significant at dilute concentrations.

Using eqs 9 and 12, t_{ind} for a diffusion-controlled process can be estimated for either a plane or a sphere. According to our model, the induction period ends when the binodal concentration for the liquid-expanded state, Γ_L is attained. Therefore, assuming that the back diffusion terms in eqs 9 and 12 are negligible and that the surface concentration at the end of the induction period is Γ_L, the length of the induction period, t_{ind} obeys

$$t_{ind} = \frac{\pi}{4D}\left(\frac{\Gamma_L}{C_\infty}\right)^2 \qquad (13)$$

for a plane and

$$\sqrt{t_{ind}} = -\frac{r_o}{\sqrt{\pi D}} + \sqrt{\frac{r_o^2}{\pi D} + \frac{\Gamma_L}{C_\infty}\frac{r_o}{D}} \qquad (14)$$

for a sphere. To estimate these quantities, Γ_L of 1.8×10^{-11} mol/cm^3 is calculated using the inverse projected area of an end-on lysozyme molecule (30 Å × 30 Å), assuming a MW of 14.3 kDa for lysozyme. A characteristic diffusion coefficient $D = 1.5 \times 10^{-6}$ cm^2/s and a bubble radius r_o of 0.08 cm are adopted. (This is the radius for a sphere with the same volume as the pendant bubble used in our experiments.)

The predicted values for t_{ind} for both the plane and the sphere are compared to those realized experimentally in Figure 12. The diffusion-controlled prediction is in reasonable agreement for dilute concentrations. However, t_{ind} realized in experiment are far longer than the predicted values at higher C_∞, indicating the presence of an adsorption kinetic barrier.

This is consistent with a shift in mechanism controlling adsorption from pure diffusion control at dilute concentration to a mixed kinetic-diffusion control at higher concentration.[7,24] To qualitatively compare the experiments at higher bulk concentrations we assume that desorption of lysozyme molecules is negligible as compared to adsorption rate. Hence the rate of accumulation of

(22) Ward, A. F. H.; Tordai, L. *J. Chem. Phys.* **1946**, *14*, 453.
(23) Miller, R.; Kretzschmer, G. *Colloid Polym. Sci* **1980**, *258*, 85.
(24) Rennan, P.; *et al. J. Colloid Interface Sci.*, in press.

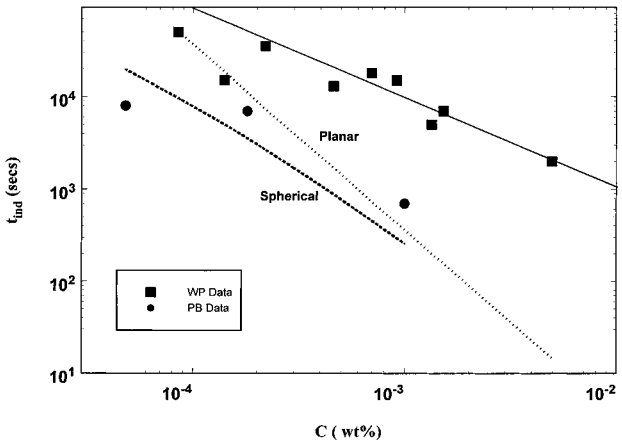

Figure 12. Plot of t_{ind} as a function of bulk lysozyme concentration. The solid line corresponds to a slope of −1, as predicted by eq 16 for a mixed kinetic−diffusion-controlled adsorption to a planar surface. The two dashed lines in the figure are the theoretical prediction for diffusion-controlled adsorption to a planar (eq 13) and spherical (eq 14) geomtery.

lysozyme molecules at the interface can be written as

$$\frac{\partial \Gamma}{\partial t} = \beta C_\infty(\Gamma_\infty - \Gamma) \tag{15}$$

where β is a kinetic constant for adsorption. Equation 15 can be integrated to give

$$t_{ind} = -\ln\left(\frac{\Gamma_\infty - \Gamma_L}{\Gamma_\infty}\right)\frac{1}{\beta C_\infty} \tag{16}$$

In a log−log plot eq 16 would be a line of slope −1. The intercept cannot be estimated because both Γ_∞ and β are unknown. A (solid) line of slope −1 is shown to pass through the high concentration Wilhelmy plate data reported in Figure 12.

4.3. Two-Component System: Suppression of the Phase Change by a Second Component. Equilibrium. Consider a monolayer formed from an insoluble amphiphile (component 1) at the interface of a solution containing a bulk soluble surface active molecule (component 2). The Frumkin adsorption isotherm adopted earlier is extended for a two-component system to relate $C_{2\infty}$ to Γ_2

$$\frac{x_2}{1 - x_1} = \frac{k}{k + \exp(K_{12}x_1 + K_{22}x_2)} \tag{17}$$

$$x_2 = \frac{\Gamma_{2eq}}{\Gamma_{2\infty}}; \quad x_1 = \frac{\Gamma_1}{\Gamma_{1\infty}}; \quad k = \frac{C_{2\infty}}{a}; \quad a = \frac{\alpha}{\beta} \tag{18}$$

and K_{12} and K_{22} are the parameters for 1−2 and 2−2 interactions, respectively; these parameters are positive for repulsive interactions and negative for cohesive ones. The corresponding equation for $\Delta\pi$ is[25]

$$\Delta\pi = \pi_{mix}(x_1,x_2) - \pi^{lipid}(x_1) = -RT\Gamma_{2\infty}\left[\ln\left(1 - \frac{x_2}{1 - x_1}\right) - K_{12}x_1x_2 - \frac{K_{22}}{2}{x_2}^2\right] \tag{19}$$

As in the single component Frumkin isotherm, the critical points can be located by equating both $\partial\Delta\pi/\partial\Gamma_2$ and $\partial^2\Delta\pi/\partial{\Gamma_2}^2$ to zero. The results are

$$K_{22} = \frac{1}{(1 - x_1 - x_{2c})^2} \tag{20}$$

where x_{2c} is determined by the positive root that is less than $(1 - x_1)$ of

$$K_{12}x_2 - \frac{x_2}{(1 - x_1 - x_2)^2} + \frac{1}{(1 - x_1 - x_2)} = 0 \tag{21}$$

Equations 20 and 21 show that the insoluble component screens the 2−2 interactions regardless of whether it interacts with the soluble amphiphile. That is, for $x_1 > 0$, the soluble component requires higher 2−2 cohesive interactions to have a phase separation for all values of K_{12}. This is illustrated in Figure 13 where $\Delta\pi$ vs $1/x_2$ is shown for $K_{22} = -6$ (strong enough cohesion to give a surface phase change for a single surfactant system) and for $K_{12} = 0$ (no 12 interactions). As the value of x_1 is increased from zero, the spinodal behavior is eliminated, and the soluble component adsorbs as a single phase. The corresponding $\Delta\pi$ vs ln k graph is also shown (see Figure 14). As x_1 increases, the cusp in this graph disappears.

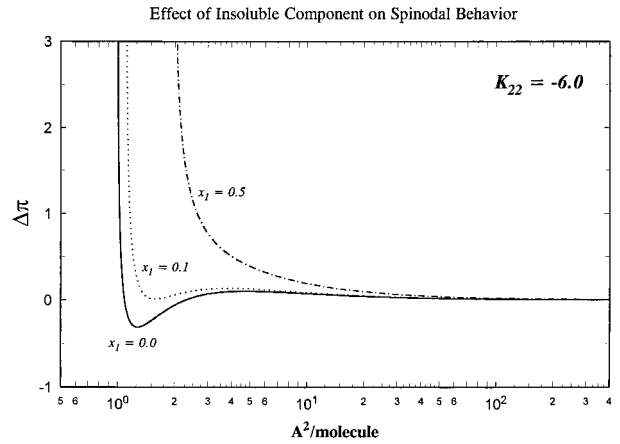

Figure 13. Plot of change in surface pressure, $\Delta\pi$, as a function of area/molecule for increasing x_1 and $K_{22} = -6$, showing that the insoluble component x_1 prevents the phase change in component 2.

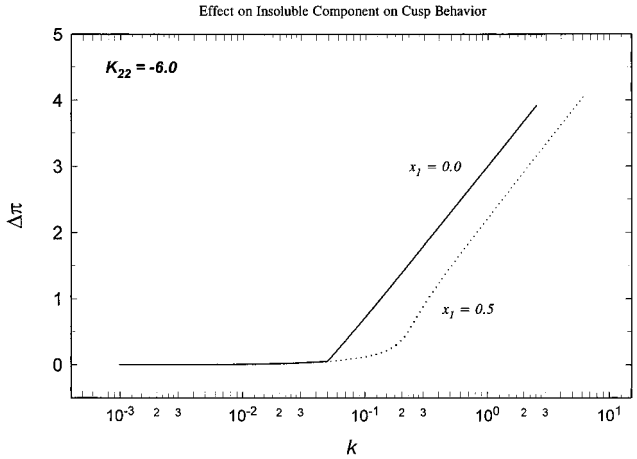

Figure 14. Plot of change in surface pressure, $\Delta\pi$, as a function of dimensionless bulk concentration, k for $K_{22} = -6.0$. As x_1 increases, the cusp disappears.

Dynamics of Monolayer Penetration: Theory. A monolayer formed from an insoluble amphiphile, (component 1) is exposed at $t = 0$ to an interface of a solution

(25) Sundaram, S.; Stebe, K. J. *Langmuir* **1996**, *12*, 2028.

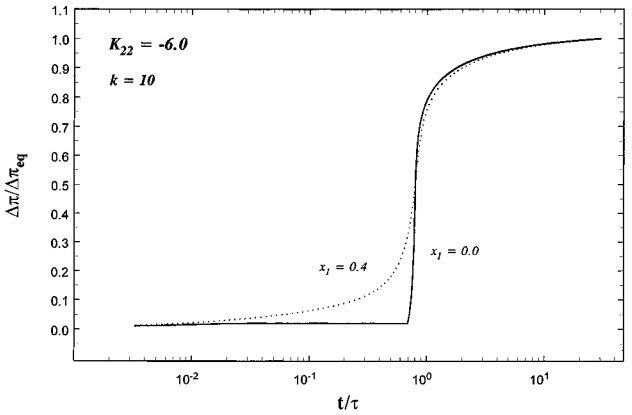

Figure 15. Plot of $\Delta\pi/\Delta\pi_{eq}$ vs t/τ (dimensionless time) as a function of x_1 and $k = 10$.

containing a bulk soluble amphiphile (component 2). Here, to illustrate how an insoluble amphiphile can effect the phase behavior of the soluble amphiphile, the components are assumed to be noninteracting and the adsorption flux to be diffusion-controlled. (The extensions to include interactions are straightforward.)

The diffusion-controlled adsorption of the soluble component into a preexisting insoluble monolayer of coverage x_1 was discussed in a previous paper.[13] The monolayer is assumed to be initially free of component 2. Diffusion establishes the instantaneous sublayer concentration. The solution to the diffusion-controlled transport of component 2 to the interface is given by eq 9.

Surfactant partitions between the sublayer and the interface according to the isotherm for $\Gamma_2 < \Gamma_{2G}$ and for $\Gamma_2 > \Gamma_{2L}$:

$$\frac{\Gamma_2(t)}{\Gamma_{2\infty}} = (1 - x_1)\left[\frac{C_{2s}(t)}{C_{2s}(t) + a\exp\left[K_{22}\dfrac{\Gamma_2(t)}{\Gamma_{2\infty}}\right]}\right] \quad (22)$$

For $\Gamma_{2G} < \Gamma_2 < \Gamma_{2L}$, the surface concentration increases to Γ_{2L} at constant diffusive flux. These equations are solved as above. Given $\Gamma_2(t)$, $\Delta\pi(t)$ is given by

$$\Delta\pi = -RT\Gamma_{2\infty}\left[\ln\left(1 - \frac{\Gamma_2(t)x_2}{\Gamma_{2eq}(1 - x_1)}\right) + K_{22}\left(\frac{\Gamma_2(t)}{\Gamma_{2eq}}x_2\right)^2\right] \quad (23)$$

for $\Gamma_2 < \Gamma_{2G}$ and for $\Gamma_2 > \Gamma_{2L}$ and by the tieline value for $\Gamma_{2G} < \Gamma_2 < \Gamma_{2L}$.

4.4. Comparison to Monolayer Penetration Data. The $\Delta\pi$ vs dimensionless time (t/τ) graphs are shown in Figure 15 as a function of x_1 for $K_{22} = -6$ and for dimensionless bulk concentration, $k = 10$. Note that as x_1 increases from zero, the plateau in the $\Delta\pi$ curve disappears. This is similar to the penetration data presented in Figure 8.

5. Isotherm and Images of Mixed Monolayers

Up to now, the effect of DPPC on the phase behavior of lysozyme has been discussed. Conversely, lysozyme also strongly alters the phase behavior of DPPC. A compression isotherm of DPPC was obtained on a lysozyme solution. DPPC was spread and compressed on the aspirated surface of a buffered lysozyme solution of concentration 1.38×10^{-4} wt % at a rate of 0.5 mm/min. This isotherm is compared to a lysozyme-free DPPC isotherm (see Figure 16; the abscissa is the area/molecule of DPPC). For the mixed monolayer, no gaseous state is

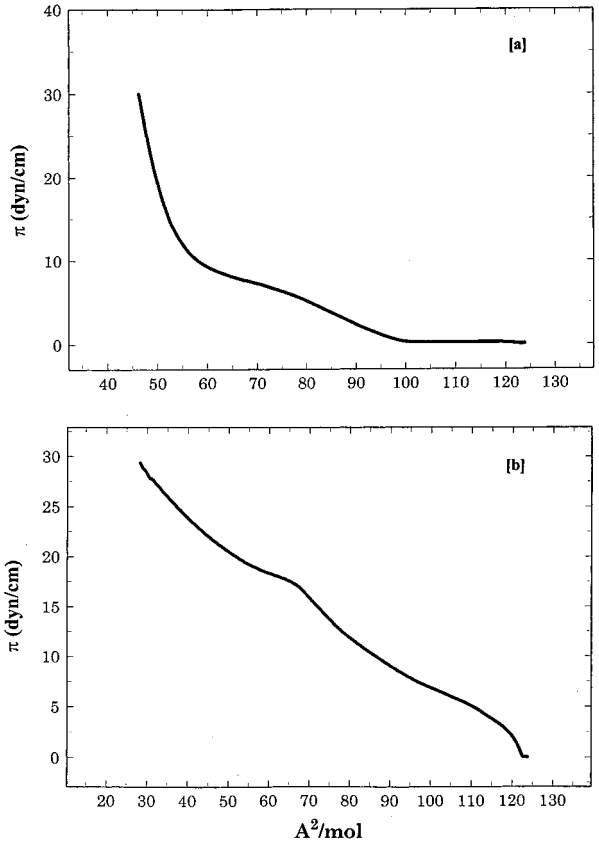

Figure 16. (a) DPPC compression isotherm on phosphate buffer saline solution. The abscissa is based on the area/molecule of DPPC. (b) DPPC compression isotherm on buffered lysozyme solution at $C = 1.38 \times 10^{-4}$ wt %. The abscissa is based on the area/molecule of DPPC.

observed. The mixed monolayer has a markedly lower compressibility at high area/DPPC molecule but greater compressibility at smaller area/DPPC molecule. Furthermore, the mixed monolayer can be compressed to areas far smaller than the choline headgroup dimensions (roughly 41A^2/molecule) which characterize the incompressible limit for a pure DPPC monolayer. This may suggest squeeze-out of the lipid from the monolayer.

The morphology and inner structure of DPPC domains formed at the aqueous−gas interface have been studied previously using BAM[20] by Vollhardt. In that study, it is reported that DPPC forms domains which have a characteristic three armed (triskelion) shape. The shape of these domains and their inner structure is dominated by the bulky DPPC headgroup. The chirality of the molecule alters both the inner and outer structure: the arms of the triskelion shape curl clockwise for *R*-DPPC and counterclockwise for *L*-DPPC. The domains have smooth variations in the intensity of the reflected light except at sharp lines that follow the shape of the arm structures. By ascertaining whether these lines remain fixed as the polarizer is adjusted, lines demarcating sharp boundaries in orientation can be differentiated from those that appear in a smoothly varying orientation. The lines within the DPPC domains indicate that the orientation varies continuously within the structures[26] (see Figure 17). Similar shapes and tilt angles are observed when DPPC is spread on buffer solution.

All experiments reported here were performed with *L*-DPPC. Chiral discrimination effects were not probed.

(26) Weidemann, G.; Vollhardt, D. *Colloid Surf.* **1995**, *100*, 187.

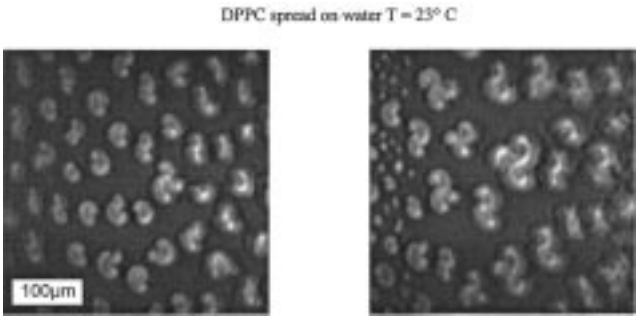

Figure 17. (a) BAM image of pure DPPC liquid condensed domains with three-arm structures and well-developed inner structure formed at the aqueous gas interface at 68 nm^2/molecule. (b) BAM image showing also the two-arm structures and domains of smaller size at the same area/molecule.

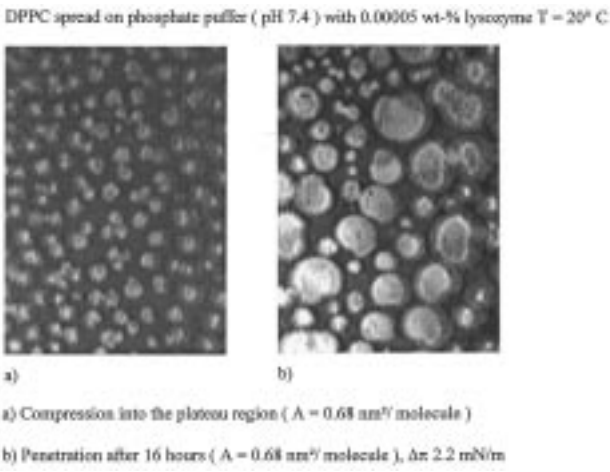

Figure 18. (a) BAM image of DPPC liquid condensed domains at 68 nm^2/molecule at the interface of a 5×10^{-5} wt % lysozyme solution immediately after compression. (b) BAM image of the same interface after being allowed to equilibrate for 16 h.

When DPPC is compressed to 68 nm^2/molecule on a subphase containing buffered lysozyme, the morphology and inner structure of the domains change remarkably (see Figure 18a). Some domains form with the triskelion shape at dilute concentrations of lysozyme (5.0×10^{-5} wt %). However, most domains are nearly circular in shape. The variation in the intensity of the reflected light is far less pronounced than in the pure DPPC domains. The monolayer was allowed to remain exposed to the lysozyme solution for 16 h (Figure 18b). The domains became densely packed, and the triskelion became more circular and uniform in tilt angle.

This effect is still more pronounced at higher concentrations of lysozyme; in Figure 19 DPPC monolayers are compressed to the same area/molecule, but exposed to 1×10^{-4} wt % lysozyme. The domains are far more densely packed on the interface, and the domain shapes are nearly circular blobs that reflect light uniformly, indicating a homogeneous tilt angle within the domains.

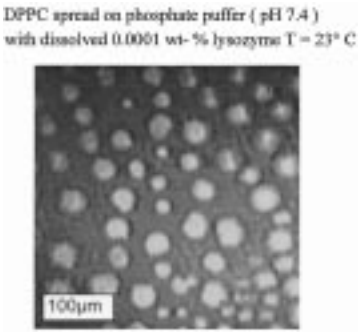

Figure 19. BAM image of DPPC liquid condensed domains at 68 nm^2/molecule at the interface of a 10^{-4} wt % lysozyme solution immediately after compression.

The shape and tilt angle of pure DPPC domains have been shown to be controlled by the phosphatidylcholine headgroup.[26] These images suggest that the structure imposed by the headgroup is disrupted by the presence of adsorbed lysozyme intercalating between the DPPC molecules.

6. Conclusions and Implications

In unison, the surface tension data, the fluorescence images in Figure 1, and the data of Hunter *et al.* establish that lysozyme undergoes a first-order phase change at the liquid−gas interface with concomitant rearrangement from side-on to end-on adsorption. Protein adsorbed in the side-on configuration is in the gaseous state, and the surface tension is relatively insensitive. The reorientation from side-on to end-on adsorption occurs at constant surface tension. The protein adsorbed in the end-on configuration is in a surface liquid-expanded state. Any additional adsorption strongly reduces the surface tension. This ability of a protein to form organized states at the interface at concentrations far below those for bulk aggregation may have implications in protein crystallization at interfaces.

Lysozyme adsorption is diffusion-controlled at dilute concentrations, kinetically controlled at higher concentrations.

The induction period disappears if lysozyme adsorbs into an insoluble monolayer. A two component Frumkin isotherm is used to discuss the suppression of the G−LE phase transition in the protein by the insoluble component. This suggests that in applications where induction periods are to be avoided, the addition of a second amphiphile can be used to eliminate them.

The system is extremely complex, in that each amphiphile alters the other's phase behavior as evidenced by BAM images and compression isotherms of the mixed monolayer.

Acknowledgment. The authors would like to thank Dr. Evangelos Moudrianakis (Biology Department, Johns Hopkins University) for providing the CD spectra of lysozyme solution. This work was partially supported by NSF Grant No. CTS9520972.

LA970670R